Structural Dynamics of Native-Like Ions in the Gas Phase:

Results from Tandem Ion Mobility of Cytochrome *c*

Samuel J. Allen, Rachel M. Eaton, Matthew F. Bush

Submitted ac-2017-012342 to *Analytical Chemistry* on April 3, 2017

Submitted ac-2017-012342.R1 to *Analytical Chemistry* on June 18, 2017

Contribution from the:

University of Washington, Department of Chemistry, Box 351700

Seattle, WA 98195-1700

*Email: mattbush@uw.edu

Abstract

Ion mobility (IM) is a gas-phase separation technique that is used to determine the collision cross sections of native-like ions of proteins and protein complexes, which are in turn used as restraints for modeling the structures of those analytes in solution. Here, we evaluate the stability of native-like ions using tandem IM experiments implemented using Structures for Lossless Ion Manipulations (SLIM). In this implementation of tandem IM, ions undergo a first dimension of IM up to a switch that is used to selectively transmit ions of a desired mobility. Selected ions are accumulated in a trap and then released after a delay to initiate the second dimension of IM. For delays ranging from 16 to 33 231 ms, the collision cross sections of native-like, 7+ cytochrome *c* ions increase monotonically from 15.1 to 17.1 nm^2. The largest products formed in these experiments at near-ambient temperature are still far smaller than those formed in energy-dependent experiments (~21 nm^2). However, the collision cross section increases by ~2% between delay times of 16 and 211 ms, which may have implications for other IM experiments on these timescales. Finally, two subpopulations from the full population were each mobility selected and analyzed as a function of delay time, showing that the three populations can be differentiated for at least 1 s. Together, these results suggest that elements of native-like structure can have long lifetimes at near-ambient temperature in the gas phase, but that gas-phase dynamics should be considered when interpreting results from IM.

Introduction

The interactions and structures of proteins and protein complexes define the complex biological functions of cells.[1] High-resolution structures of proteins can be determined using x-ray crystallography, but the process for successful structural determination can be interrupted at each step between purifying the sample and solving the diffraction data.[2] Ion mobility (IM) mass spectrometry (MS) has emerged as a powerful technique for characterizing the structures and assemblies of biological systems. Electrospray ionization of proteins from buffered solutions at biologically relevant pH results in gas-phase ions that can retain noncovalent interactions similar to those in solution,[3,4] and are often referred to as "native-like". IM separates ions based on their electrical mobility in a neutral gas and is sensitive to the sizes and shapes of ions. The mobility of an ion depends on its charge state and collision cross section (Ω) value which, to the first approximation, depends on the orientationally-averaged projected area of the ion-neutral gas pair.[5,6] Pairing IM with MS enables rapid characterization of the shapes and masses of ions. IM-MS analysis has been used to characterize numerous biomolecules and bimolecular assemblies, including those that are membrane bound[7,8] and intrinsically disordered.[9,10]

Clemmer and coworkers pioneered the use of IM-IM-MS, which is also called tandem IM, to evaluate the stability and structural diversity of gas-phase ions. Their tandem IM measurements were performed by joining two ~1 m long stacked-ring drift tubes.[11] In this design, a first dimension of IM separation is performed in the first drift tube. The end of the first drift tube contains an ion funnel,[12] which selectively transmits or omits ions depending on their drift time, or mobility. Mobility-selected ions are then transmitted into the second drift tube for a second dimension of IM separation. Seminal work using this instrument showed that the selection of narrow drift time ranges from the broad arrival-time distribution of 7+ ubiquitin

yields discrete structures that are stable on the millisecond timescale of the separation.[13] That work and other examples of multidimensional IM,[14–16] IM filtering,[17] and high IM resolution[18] provide a growing body of evidence supporting the conclusion that broad IM distributions are the consequence of ensembles of stable structures.

The stability of native-like ion structures within the timescale of most IM-MS experiments remains uncertain. Breuker and McLafferty proposed a timeline for the structural changes of a protein ion after transfer from the solution to gas phase, based on meta-analysis of experimental and theoretical results.[19] Following the complete desolvation of a protein ion after ionization, new ionic bonds form between the desolvated charged residues on the picosecond timescale, according to molecular dynamics simulations.[20] These ionic bonds are capable of holding the native-like structure intact for milliseconds. However, given the loss of the hydrophobic effect concomitant with desolvation, van der Waals and other weak interactions will be lost over time in favor of the formation of stronger noncovalent interactions. Within seconds to minutes, sufficient protein unfolding may occur such that the protein can refold to a more stable gas-phase structure. Evidence of partial unfolding and refolding has been observed for a number of proteins, including ubiquitin[15,21–23] and cytochrome *c*.[24–26] A detailed understanding of the stability of native-like ions under the conditions and timescales of IM separations is lacking and crucial for advancing native IM-MS.

Here, we investigate the stability of native-like, cytochrome *c* ions at near-ambient temperature using a recently introduced IM technology, Structures for Lossless Ion Manipulations (SLIM).[27,28] The goal of this work is to characterize the structures of native-like ions in terms of (1) their stability over typical (16 to 211 ms) and extended (~33 s) IM timescales and (2) the dynamics of structural subpopulations from the initial ensemble of ions. These

investigations are enabled by tandem IM, which is used to select populations of native-like ions and to monitor their structures as a function of residence time under near-ambient temperatures.

Methods

Sample Preparation and Ionization. Cytochrome *c* from equine heart was purchased from Sigma-Aldrich (St. Louis, MO, P/N C2506). Ions were generated using electrokinetic, nanoelectrospray ionization[29] from solutions containing 10 μM cytochrome *c* in 200 mM ammonium acetate at pH 7.0.

Instrumentation. The instrument used for these experiments is similar to that reported previously,[30] but with modifications to enable tandem IM prior to MS as described below. This instrument uses Structures for Lossless Ion Manipulations (SLIM) technology (Figures 1a and 1b), in which planar electrodes are deposited directly onto printed circuit boards that deliver DC and RF potentials.[27,28] Pairs of 7.62 x 7.62 cm SLIM boards, with a 3.97 mm board-to-board distance, form modules that can be combined into different arrays to enable additional experiments. Ions from electrospray were introduced into the first vacuum chamber, where they were accumulated in an ion funnel trap.[31] The ion funnel trap injects a packet of ions into the second vacuum chamber, which contains a rectangular ion funnel,[32] six SLIM modules, and a circular ion funnel.[33] The first and second chambers were operated at pressures of ~3.99 and ~4.04 Torr nitrogen gas, respectively. The DC electric fields in the post-trapping region of the ion funnel trap, the rectangular ion funnel, the SLIM modules (excluding the orthogonal path described below), and the circular ion funnel were 14, 4, 4, and 8 V cm^{-1}, respectively. IM separated ions were detected using a Waters Q-Tof Premier mass spectrometer and an

independent analog-to-digital converter.[30] Additional instrument details are described in the Supporting Information.

Determining *Ω* Values using SLIM. No traveling waves are used in this implementation of SLIM. Instead, ions are separated using a constant DC gradient (Figure 1c), which is analogous to electrostatic drift tubes and RF-confining drift cells.[34] The drift velocity (v_D) of these ions depends on their mobility (K) under an applied electric field (E):

$$v_D = KE \tag{1}$$

Voltage-dependent measurements were conducted to determine K values and the transport times outside the SLIM drift region. Ω values were then determined using the Mason-Schamp equation:[5]

$$\Omega = \frac{3ez}{16N}\left(\frac{2\pi}{\mu k_B T}\right)^{1/2}\frac{1}{K} \tag{2}$$

where e is the elementary charge, z is the ion charge state, N is the drift-gas number density, μ is the reduced mass of the ion and drift gas, k_B is the Boltzmann constant, and T is the drift-gas temperature (300 K).

Tandem IM. Initially, ions were accumulated and ejected from an ion funnel trap (see Supporting Information for details). Packets of ions pass through three linear modules prior to entering a tee module (position 4, Figure 1d), which selects ions with desired drift times through the first dimension. Tee boards contain a linear array of electrodes to transmit ions along a straight path, and an orthogonal array of electrodes to transmit ions that are diverted from the path of transmission.[35,36] Mobility filtering is performed by applying DC potentials to two "switch guard" electrodes near the intersection of the two paths, which were programmed to selectively transmit or divert ions of selected drift times. The straight and orthogonal paths were held at 4 and 8.4 V cm^{-1}, respectively. For all mobility selection experiments, the switch guard

voltages were increased by 30 V to divert ions toward the orthogonal path. The time during which the switch guard voltages were held low to transmit ions along the collinear path will be referred to as the "transmission window" (Figure 2a).

In addition to the selection of specific drift times, packets of transmitted ions can also be accumulated in the "junction trap" between modules 4 and 5 (Figure 1d). Trapping was performed by biasing the DC voltage of the first electrodes of module 5 by +10 V relative to the DC voltage of the final electrodes on module 4 (Figure S1). The bias voltage was decreased to release the ion packet from the junction trap and then raised by +10 V prior to the next ion packet arriving at the switch. A summary of the trapping parameters and times are shown in Figure 2a. Experiments in which selection and junction trapping are performed will be referred to as "selection-trapping" experiments. Ω values from selection-trapping experiments were determined using a method similar to that described above for single dimensional experiments that is described further in the Supporting Information.

Ion Trajectory Simulations and Effective Temperatures. Ion trajectories of 7+ cytochrome *c* were simulated in SIMION[37] 8.1 using the HS1 hard-sphere approximation for elastic ion-neutral collisions. The mean free path of 7+ cytochrome *c* was estimated using the Ω value reported previously.[30] Models of SLIM used 4 Torr nitrogen gas and electrode dimensions reported previously.[30] The effective translational temperatures of ions were estimated using results from ion trajectory simulations and a recently introduced statistical approach[34] that is described in the Supporting Information.

Collision-Induced Unfolding (CIU). CIU experiments were performed on a Waters Synapt G2 HDMS in which the traveling-wave ion mobility cell was replaced with an RF-confining drift cell.[38] Ions were accelerated into the Trap Cell containing argon gas (3.5×10^{-2}

mbar) using varying injection voltages. Drift times were measured post-activation using the RF-confining drift cell operated at a drift voltage of 138 V in either 0.50 Torr nitrogen gas or 1.72 Torr helium gas. Drift times were converted to Ω values using results from voltage-dependent measurements[38] and Equation 2.

Results and Discussion

A detailed understanding of the stability and dynamics of native-like ions during IM-MS experiments it critical for advancing native IM-MS and maximizing the information content of those experiments. Towards that end, energy-dependent, single-dimensional IM experiments were used to probe conformational landscape of native-like, 7+ cytochrome *c*. Time-dependent, tandem IM experiments, which are enabled by a new instrument platform, were then used to probe the dynamics of those ions and isolated subpopulations under near-ambient temperatures.

IM-MS of Cytochrome *c*. Cytochrome *c* ions were produced from aqueous solutions containing 200 mM ammonium acetate at pH 7.0 and analyzed using an RF-confining drift cell with a low pressure (0.5 Torr) of nitrogen gas and injection voltages near the threshold for ion transmission. The resulting distribution of Ω with nitrogen of the 7+ ion is shown in Figure 3a (4 V trace). The median value of this distribution is 15.3 nm^2, which is similar to that determined using a previous RF-confining drift cell (15.9 nm^2).[39] Most Ω values determined in this work were measured with nitrogen gas and, therefore, are systematically larger than those measured with helium gas due to differences in effective van der Waals radii, polarizabilities, and other factors.[39,40] Note that a previous measurement using this RF-confining drift cell yielded a value of 19.7 nm^2, which was attributed to activation during injection into a higher pressure of nitrogen gas (1.0 Torr).[30] These results indicate that the current experiments probe compact

conformations. Compact Ω values such as this are consistent with "native-like" structures that can correlate well with Ω values calculated from crystal structures,[41,42] although compact Ω values that are smaller than expected for the native structures have also been reported in some cases.[9,43]

The potential-energy surface of protein ions in the gas phase can be probed using collision-induced unfolding (CIU), in which the internal energies of ions are increased through collisional activation with neutral, inert gases prior to re-thermalization. Results from CIU experiments show that it is possible to form stable, unfolded conformations at increasing injection voltages into a collision cell.[44,45] CIU of 7+ cytochrome *c* is shown in Figure 3b, plotted as a heat map of Ω versus injection voltage. The medians of the Ω distributions are shown as a dashed line in Figure 3b and were determined from the corresponding cumulative distribution functions (CDF, Figure S2). Briefly, the CDF is the probability of the distribution's density, *e.g.*, the Ω at which the CDF has a value of 50% corresponds to median of the Ω distribution. The initial Ω distribution is stable up to an injection voltage of 10 V and then gradually increases in magnitude and width with increasing injection voltage. At injection voltages of at least 25 V, a distribution centered near ~21 nm^2 is the dominant feature. The persistence of similar Ω distributions with increasing energy is consistent with the formation of gas-phase-annealed structures that have reached a quasi-equilibrium.[46] For comparison, the Ω distributions measured at injection voltages of 4, 20, and 40 V are plotted in Figure 3a. These distributions show the changes in Ω values resulting from CIU, and serve as points-of-reference for the time-dependent data discussed later.

The Ω distribution of 7+ cytochrome *c* determined here using SLIM is shown in Figure 3a, which is similar to that determined using the RF-confining drift cell under low-energy

conditions. This implementation of SLIM does not use traveling waves; a constant DC gradient separates ions longitudinally (Figure 1c) based on Equation 1 and yields Ω values that are similar to those determined using other ion mobility devices for native IM-MS.[30] The apparent resolving powers of the Ω distributions shown in Figure 3a are 10.4 and 11.8 for measurements performed in an RF-confining drift cell or SLIM, respectively. The improved performance of SLIM-based measurement is primarily due to the longer drift time (~80 ms in SLIM versus ~4 ms in an RF-confining drift cell), which reduces the relative contributions of gating.[30] These results suggest that the initial native-like ions probed on both platforms are similar.

IM-IM-MS of Cytochrome *c*. We expanded the capabilities of our SLIM instrument by implementing modules to perform IM-IM-MS (tandem IM) of native-like ions. In these tandem IM experiments, native-like ions were selected and trapped as a function of time to investigate their stability at near-ambient temperature. In the first dimension of IM, ions were separated as they were transported from the initial trapping region to the switch (Figure 1d). Time-dependent potentials were used to selectively transmit or divert ions, as a function of their drift time as they entered the switch. For the initial experiments, a 7.125 ms transmission window was used to transmit all 7+ cytochrome *c* ions, and, consequently, divert all other ions down the orthogonal path to a collection electrode. Next, the transmitted ions were accumulated in the junction trap between modules 4 and 5 using a bias potential of +10 V (Figure S1). After a delay, ions released from the junction trap underwent a second dimension of IM separation through two linear modules and a circular ion funnel.

Figure 4 (bottom trace) shows tandem IM of 7+ cytochrome *c* using a 16 ms delay between selection and the beginning of the second dimension of IM analysis. This is the first demonstration of tandem IM of a native-like ion using SLIM. The residence time of ions in the

junction trap depends on (1) the delay time, which is defined in Figure 2a, and (2) the transport time from the switch to the junction trap. The average transport time for these ions is ~4.6 ms, which is shorter than the delay time. The Ω distributions acquired in single-dimensional IM (Figure 3a) experiments and selection-trapping experiments with short delays are similar. That is, ions trapped during short delay times do not undergo resolvable structural changes. The delay time was varied up to 33 231 ms. The resulting Ω distributions are shown in Figure 4a and exhibit a monotonic increase in Ω with increasing delay time. The maximum delay time is limited by charge-stripping of the 7+ ions (Figure S3), which has been observed for native-like ions during other long-timescale experiments[47] and is discussed in the Supporting Information.

Figure 4b shows the median Ω values as a function of the delay time. These results demonstrate that the median values increase by 13% over the entire range of delay times, but that the rate of Ω change decreases considerably with increasing delay time. Most notably, there is a significant increase in median Ω for each increase in delay time from 16 to 991 ms, which spans the range of timescales of essentially all IM experiments.[18,48,49] For comparison, there is a 64.5 ms delay between the beginning of the first and second dimensions in experiments using a 16 ms delay time (Figure 2) and the drift time in the second dimension is ~28 ms. These results indicate that the structures of native-like, 7+ cytochrome *c* ions are not static during these and other native IM-MS experiments. Although the increase in Ω values between delay times of 16 to 211 ms is only ~2%, that difference is remarkably similar to the uncertainties reported for several IM instruments used for structural applications.[38,48,50] This suggests that small differences in Ω values reported for native-like ions may be partially attributable to structural dynamics occurring over the various timescales of IM instruments.

The energy-dependent (Figure 3) and time-dependent (Figure 4) experiments both probe the structural evolution of cytochrome *c* ions in the gas-phase and exhibit evidence for the appearance of ions with larger *Ω*. Interestingly, ions in the time-dependent experiments exhibit an immediate change in *Ω* values with small increases in delay time, whereas ions in the CIU experiments exhibit an induction period in which initial increases in injection energy do not result in increases in *Ω*. Note that ions in CIU experiments can achieve far higher internal energies than ions trapped at near-ambient temperature, but the activated ion lifetimes in the former are far shorter than the delay times of the latter. Therefore, different isomerization pathways may be accessed in the two experiments. That is, although activation in both experiments is relatively slow[51] and will favor pathways with low barriers to isomerization, ions in the CIU experiments are more likely to proceed through entropically favorable short cuts towards lower-energy structures. Characterizing these differences will be the subject of future investigations. Finally, the range of *Ω* values in tandem IM experiments (Figure 4b) is smaller than those observed in CIU experiments. The largest median *Ω* value measured in tandem IM experiments is 17.1 nm^2, which is similar to the intermediate *Ω* distribution measured at 16 V in CIU experiments. This indicates that the ions in the former experiments have not reached an equilibrium (or quasi-equilibrium) ensemble of structures, even after 30 s in the gas phase.

Effective Temperatures. The internal energies of the ions in these tandem IM experiments were estimated using a recently introduced statistical approach[34] and ion trajectory simulations. Using this method, the effective translational temperature of 7+ cytochrome *c* in SLIM operated at 4 V cm^{-1} and 4 Torr nitrogen, without junction trapping, is 299.9 K. This temperature is similar to that estimated previously for native-like avidin ions in SLIM (~299 K) using this method,[30] and that calculated for 7+ cytochrome *c* in an electrostatic drift tube (300.4

K) based on the drift-gas temperature and drift velocity of the ion.[52] Using the statistical approach, an effective translational temperature of 308.4 K was estimated for 7+ cytochrome *c* held in the junction trap with a bias of +10 V and a pre-switch field strength of 4 V cm^{-1} (Figure S4), which is slightly higher than that for ions not held in the junction trap. Note, the internal energy of the ions also depends on how efficiently energy is converted between the translational and internal degrees of freedom. Therefore, temperatures estimated here are the upper limit of the effective vibrational temperatures of these ions.[34] These results all suggest that the internal energies of the ions in the tandem IM experiments are similar to those expected at ambient temperature.

Comparisons to Previous Experiments. Jarrold, Clemmer, and coworkers used a series of pioneering IM experiments to probe the structures and stabilities of 7+ cytochrome *c* produced from 49/49/2 water/methanol/acetic acid solutions. Those results indicate that those ions populate distinct structural distributions that they refer to as states A to E, in order of increasing Ω with helium.[53,54] For comparison, the Ω values of 7+ cytochrome *c* after CIU were measured in helium gas using an RF-confining drift cell (Figure S5). Under low-energy conditions, Ω values of native-like 7+ cytochrome *c* are consistent with state A. As those ions are activated, there is a gradual change in Ω value that is consistent with sequential transitions from A to D, with D favored in the gas-phase-annealed population. Interestingly, no evidence for the E state was observed in these CIU experiments, even under the highest-energy conditions.

Clemmer and coworkers observed increases in Ω for ions that were held in a Paul trap (10^{-4} to 10^{-3} Torr He) as a function of time prior to IM-MS analysis.[21,25,54] Most relevant to this work, the arrival-time distributions of 7+ cytochrome *c* (produced from 49/49/2 water/methanol/acetic acid solutions) were measured for trapping times up to 71 ms.[54] For

increasing trapping times from 31 to 71 ms, the intensity of the feature for the compact state A decreases whereas those for states B and C increase. The appearance of structures with larger Ω in that study[54] may be analogous to the shift in Ω distribution observed in Figure 4. Qualitative comparison of the CIU plots of ions measured in helium gas (Figure S5) to those measured in nitrogen gas (Figure 3b) suggest that native-like 7+ cytochrome *c* ions may transition from state A to B for delay times ranging from 16 to 33 231 ms in Figure 4.

To compare the rates of change in the current and previous time-dependent experiments, unimolecular unfolding rates were estimated for the depletion of the initial Ω distribution in the present experiments (Figure 5). Analogous to rate of change of the median Ω in Figure 4, the depletion of the initial population is consistent with two different kinetic rates; a faster rate of 0.31 s^{-1} at delay times ranging from 16 to 991 ms and a slower rate of 0.042 s^{-1} for the longer delay times. Note that it is also possible that the slower depletion rate is the results of interference with depletion products. Both of these rates are far slower than that for the depletion of state A in the Paul trap experiments (40 s^{-1}).[54] One possibility is that the effective temperature of the ions stored in the Paul trap was greater than that for ions stored in the junction trap in the present experiments (~308 K, see above), although those authors propose that the ions stored in their Paul trap would equilibrate to the gas temperature of 300 K.[54] Alternatively, although the initial ions generated from denaturing and native-like conditions appear to exhibit similar Ω_{He} (Figure S5), it is possible that they have different structures and stabilities in the gas phase. This possibility is consistent with differences in the CIU patterns observed for 7+ cytochrome *c* generated from different solutions (Figure S5).

Isolation of Subpopulations. The apparent Ω distribution of native-like, 7+ cytochrome *c* ions determined using tandem IM and a 16 ms delay time is shown in Figure 6a (bottom panel,

shaded distribution). The apparent resolving power of that distribution is 9.7, which is lower than that for the single-dimensional analysis (11.8) due to the lower absolute voltage used over the shorter path length of the second dimension. However, this distribution is still very broad compared to the diffusion-limited[55] width at base expected for a single structure under these conditions (0.69 nm^2), which is consistent with the entire population (labeled **I**) containing an ensemble of structures.[13,38] Note that the contribution from gating appears to be much smaller than that from diffusion in this implementation, which will be reported in detail separately.

Two subpopulations from population **I** were each selected individually and analyzed using a ~16 ms delay time (bottom panel of Figure 6a). Those selections used transmission windows of 1.125 ms that differed in absolute time by 2.25 ms. Subpopulation **II** spans a range of more compact Ω values than subpopulation **III**. Note that there is a 64.5 ms delay between the beginning of the first dimension and the beginning of the second dimension for the analysis of populations **I**, **II**, and **III**, as depicted in Figure 2b. The actual time differences between ion selection and the beginning of the second dimension differ by up to 2 ms in the three experiments, depending on the mobilities of the ions. For simplicity, a common delay time (Figure 2b) is reported for experiments probing the three populations. The Ω distributions for the two subpopulations are clearly different, but are each broader than expected for a single conformer (0.69 nm^2 width at base). This result is consistent with inadequate separation of conformers during the first dimension of IM, transmission of multiple separated conformers, and/or isomerization during the 16 ms delay.

Structural Evolution of Subpopulations. Using the same transmission windows, the apparent Ω distributions resulting from selection-trapping experiments with delay times up to 8271 ms were determined and are included in Figure 6a. Similar to the results for the entire

population (Figure 4), subpopulations **II** and **III** exhibit a gradual increase in apparent Ω values with increasing delay times. Initially, each subpopulation exhibits different apparent Ω distributions. With increasing delay times, subpopulations **II** and **III** become increasingly similar to each other and population **I**.

To quantitatively evaluate the Ω distributions, Figure 6b shows the median Ω values as a function of the fourth root of delay time, which was chosen arbitrarily to aid in visualization. The median Ω values for the three populations all increase to larger Ω values with increasing delay time, and the Ω values of **I**, **II**, and **III** differ from each other for up to a second in the gas-phase before isomerizing to indistinguishable populations. Additionally, comparing the best fit lines through the average values measured at a delay time of 8271 ms shows that the more compact initial subpopulation (**II**) isomerizes at a faster rate than the original population (**I**), which in turn isomerizes faster than the less compact initial subpopulation (**III**). Figure 6c shows the average width of the Ω distributions as a function of delay time. Initially, the widths of the Ω distributions for the two subpopulations are similar to each other and smaller than that for the entire population. With increasing delay time, the widths of each population increase and become indistinguishable for delay times of at least 2 s, based on the standard error of the measurements. Using kinetic models to interpret the structural evolution of different ion populations will be the subject of future investigations. More generally, Figure 6 shows that the gas-phase dynamics of these native-like ions depend on the initial population of structures, which suggests that native-like ions can retain some memory of subtle details of their initial gas-phase structures for at least 1 s in the gas phase at ambient temperature.

Conclusions

The structures and stabilities of native-like, 7+ cytochrome *c* were probed using energy-dependent and time-dependent experiments. Initially, the native-like ions in these experiments exhibit median Ω near 15 nm^2 (Figure 3a). In energy-dependent experiments, a wide range of high-energy conditions yield similar Ω distributions with maxima near 21 nm^2 (Figure 3b). The persistence of similar Ω distributions with increasing energy is consistent with the formation of gas-phase-annealed structures that have reached a quasi-equilibrium.[46] In time-dependent experiments enabled by a new tandem IM instrument, the Ω distributions increase monotonically for delay times ranging from 16 to 33 231 ms (Figure 4). Although the median Ω values increase with time, the median value after the longest delay is only ~17.1 nm^2, which is far smaller than that for the gas-phase annealed structures. Two subpopulations from the initial ensemble were isolated and analyzed as a function of delay time (Figure 6a). Comparison of the resulting Ω distributions shows that the medians (Figure 6b) and widths (Figure 6c) of the subpopulations evolve at different rates than the full population, and that each of the three populations can be differentiated for at least 1 s.

The time-dependent results show that native-like ions evolve on the tens of milliseconds timescale (Figure 4b), which is comparable to the timescale of many IM separations.[18,48,49] Although the increase in Ω value between delay times of 16 to 211 ms is only ~2%, this increase is comparable to the uncertainties reported for several IM instruments used for structural applications.[38,48,50] Thus, these structural transitions likely occur during other IM experiments, but would be very difficult to isolate in a single-dimensional IM analysis without independent control of time. The rate of change in Ω (Figure 4b) and the rates of depletion of the initial structural population (Figure 5) decreases with increasing delay time. Notably, the rates of

depletion of the initial structural population of native-like, 7+ cytochrome *c* (0.31 and 0.042 s^{-1}) are far slower than that reported for 7+ cytochrome *c* generated from 49/49/2 water/methanol/acetic acid solutions (40 s^{-1}).[54] These results suggest that after the initial isomerization events, compact structures with significant memory of the initial native-like structures can have long lifetimes in the gas phase at near-ambient temperature.

Acknowledgements. This material is based upon work supported by the National Science Foundation under CHE–1550285 (M. F. B.) and DGE-1256082 (R. M. E.), and Eli Lilly and Company (Young Investigator Award in Analytical Chemistry to M. F. B.). We thank the SLIM Consortium at Pacific Northwest National Laboratory, including Dr. Richard Smith, Dr. Yehia Ibrahim, Dr. Randy Norheim, Dr. Tsung-Chi Chen, Spencer Prost, and Dr. Ian Webb for sharing designs, software, and technical expertise. We thank Gordon Anderson (GAA Custom Engineering) for assistance with electronics.

Supporting Information Available.

This material is available free of charge via the Internet at http://pubs.acs.org.

Additional instrument details, determining Ω values using tandem IM, effective temperature statistical analysis, charge-stripping discussion, and Figures S1 to S5.

References

(1) Marsh, J. A.; Teichmann, S. A. *Annu. Rev. Biochem.* **2015**, *84*, 551–575.
(2) Stacy, R.; Begley, D. W.; Phan, I.; Staker, B. L.; Van Voorhis, W. C.; Varani, G.; Buchko, G. W.; Stewart, L. J.; Myler, P. J. *Acta Cryst. Sect. F* **2011**, *67*, 979–984.
(3) Benesch, J. L. P.; Ruotolo, B. T.; Simmons, D. A.; Robinson, C. V. *Chem. Rev.* **2007**, *107*, 3544–3567.
(4) Leney, A. C.; Heck, A. J. R. *J. Am. Soc. Mass Spectrom.* **2017**, *28*, 5–13.
(5) Mason, E. A.; McDaniel, E. W. *Transport Properties of Ions in Gases*, pg. 276.; Wiley: New York, 1988.
(6) Wyttenbach, T.; Bleiholder, C.; Bowers, M. T. *Anal. Chem.* **2013**, *85*, 2191–2199.
(7) Zhou, M.; Politis, A.; Davies, R. B.; Liko, I.; Wu, K.-J.; Stewart, A. G.; Stock, D.; Robinson, C. V. *Nat. Chem.* **2014**, *6*, 208–215.
(8) Laganowsky, A.; Reading, E.; Allison, T. M.; Ulmschneider, M. B.; Degiacomi, M. T.; Baldwin, A. J.; Robinson, C. V. *Nature* **2014**, *510*, 172–175.
(9) Pagel, K.; Natan, E.; Hall, Z.; Fersht, A. R.; Robinson, C. V. *Angew. Chem. Int. Ed.* **2013**, *52*, 361–365.
(10) Jurneczko, E.; Cruickshank, F.; Porrini, M.; Clarke, D. J.; Campuzano, I. D. G.; Morris, M.; Nikolova, P. V.; Barran, P. E. *Angew. Chem. Int. Ed.* **2013**, *52*, 4370–4374.
(11) Koeniger, S. L.; Merenbloom, S. I.; Valentine, S. J.; Jarrold, M. F.; Udseth, H. R.; Smith, R. D.; Clemmer, D. E. *Anal. Chem.* **2006**, *78*, 4161–4174.
(12) Tang, K.; Shvartsburg, A. A.; Lee, H.-N.; Prior, D. C.; Buschbach, M. A.; Li, F.; Tolmachev, A. V.; Anderson, G. A.; Smith, R. D. *Anal. Chem.* **2005**, *77*, 3330–3339.
(13) Koeniger, S. L.; Merenbloom, S. I.; Clemmer, D. E. *J. Phys. Chem. B* **2006**, *110*, 7017–7021.
(14) Merenbloom, S. I.; Koeniger, S. L.; Valentine, S. J.; Plasencia, M. D.; Clemmer, D. E. *Anal. Chem.* **2006**, *78*, 2802–2809.
(15) Koeniger, S. L.; Clemmer, D. E. *J. Am. Soc. Mass Spectrom.* **2007**, *18*, 322–331.
(16) Simon, A.-L.; Chirot, F.; Choi, C. M.; Clavier, C.; Barbaire, M.; Maurelli, J.; Dagany, X.; MacAleese, L.; Dugourd, P. *Rev. Sci. Instrum.* **2015**, *86*, 094101.
(17) Kurulugama, R. T.; Nachtigall, F. M.; Lee, S.; Valentine, S. J.; Clemmer, D. E. *J. Am. Soc. Mass Spectrom.* **2009**, *20*, 729–737.
(18) Merenbloom, S. I.; Glaskin, R. S.; Henson, Z. B.; Clemmer, D. E. *Anal. Chem.* **2009**, *81*, 1482–1487.
(19) Breuker, K.; McLafferty, F. W. *Proc. Natl. Acad. Sci. U. S. A.* **2008**, *105*, 18145–18152.
(20) Steinberg, M. Z.; Elber, R.; McLafferty, F. W.; Gerber, R. B.; Breuker, K. *ChemBioChem* **2008**, *9*, 2417–2423.
(21) Myung, S.; Badman, E. R.; Lee, Y. J.; Clemmer, D. E. *J. Phys. Chem. A* **2002**, *106*, 9976–9982.
(22) Skinner, O. S.; McLafferty, F. W.; Breuker, K. *J. Am. Soc. Mass Spectrom.* **2012**, *23*, 1011–1014.
(23) Laszlo, K. J.; Munger, E. B.; Bush, M. F. *J. Am. Chem. Soc.* **2016**, *138*, 9581–9588.
(24) Breuker, K.; McLafferty, F. W. *Angew. Chem. Int. Ed.* **2003**, *42*, 4900–4904.
(25) Badman, E. R.; Myung, S.; Clemmer, D. E. *J. Am. Soc. Mass Spectrom.* **2005**, *16*, 1493–1497.

(26) Laszlo, K. J.; Buckner, J. H.; Munger, E. B.; Bush, M. F. *J. Am. Soc. Mass Spectrom.* **2017**, DOI: 10.1007/s13361-017-1620-4.
(27) Tolmachev, A. V.; Webb, I. K.; Ibrahim, Y. M.; Garimella, S. V. B.; Zhang, X.; Anderson, G. A.; Smith, R. D. *Anal. Chem.* **2014**, *86*, 9162–9168.
(28) Webb, I. K.; Garimella, S. V. B.; Tolmachev, A. V.; Chen, T.-C.; Zhang, X.; Norheim, R. V.; Prost, S. A.; LaMarche, B.; Anderson, G. A.; Ibrahim, Y. M.; Smith, R. D. *Anal. Chem.* **2014**, *86*, 9169–9176.
(29) Davidson, K. L.; Oberreit, D. R.; Hogan, C. J.; Bush, M. F. *Int. J. Mass Spectrom.* **2017**, DOI: 10.1016/j.ijms.2016.09.013.
(30) Allen, S. J.; Eaton, R. M.; Bush, M. F. *Anal. Chem.* **2016**, *88*, 9118–9126.
(31) Clowers, B. H.; Ibrahim, Y. M.; Prior, D. C.; Danielson, W. F.; Belov, M. E.; Smith, R. D. *Anal. Chem.* **2008**, *80*, 612–623.
(32) Chen, T.-C.; Webb, I. K.; Prost, S. A.; Harrer, M. B.; Norheim, R. V.; Tang, K.; Ibrahim, Y. M.; Smith, R. D. *Anal. Chem.* **2015**, *87*, 716–722.
(33) Ibrahim, Y. M.; Baker, E. S.; Danielson III, W. F.; Norheim, R. V.; Prior, D. C.; Anderson, G. A.; Belov, M. E.; Smith, R. D. *Int. J. Mass Spectrom.* **2015**, *377*, 655–662.
(34) Allen, S. J.; Bush, M. F. *J. Am. Soc. Mass Spectrom.* **2016**, *27*, 2054–2063.
(35) Webb, I. K.; Garimella, S. V. B.; Tolmachev, A. V.; Chen, T.-C.; Zhang, X.; Cox, J. T.; Norheim, R. V.; Prost, S. A.; LaMarche, B.; Anderson, G. A.; Ibrahim, Y. M.; Smith, R. D. *Anal. Chem.* **2014**, *86*, 9632–9637.
(36) Garimella, S. V. B.; Ibrahim, Y. M.; Webb, I. K.; Ipsen, A. B.; Chen, T.-C.; Tolmachev, A. V.; Baker, E. S.; Anderson, G. A.; Smith, R. D. *Analyst* **2015**, *140*, 6845–6852.
(37) Dahl, D. *SIMION* version 8.1; Idaho National Engineering Laboratory: Idaho Falls, ID.
(38) Allen, S. J.; Giles, K.; Gilbert, T.; Bush, M. F. *Analyst* **2016**, *141*, 884–891.
(39) Bush, M. F.; Hall, Z.; Giles, K.; Hoyes, J.; Robinson, C. V.; Ruotolo, B. T. *Anal. Chem.* **2010**, *82*, 9557–9565.
(40) Bleiholder, C.; Johnson, N. R.; Contreras, S.; Wyttenbach, T.; Bowers, M. T. *Anal. Chem.* **2015**, *87*, 7196–7203.
(41) Jurneczko, E.; Barran, P. E. *Analyst* **2010**, *136*, 20–28.
(42) Bereszczak, J. Z.; Barbu, I. M.; Tan, M.; Xia, M.; Jiang, X.; van Duijn, E.; Heck, A. J. R. *J. Struct. Biol.* **2012**, *177*, 273–282.
(43) Hall, Z.; Politis, A.; Bush, M. F.; Smith, L. J.; Robinson, C. V. *J. Am. Chem. Soc.* **2012**, *134*, 3429–3438.
(44) Ruotolo, B. T.; Hyung, S.-J.; Robinson, P. M.; Giles, K.; Bateman, R. H.; Robinson, C. V. *Angew. Chem. Int. Ed.* **2007**, *46*, 8001–8004.
(45) Freeke, J.; Bush, M. F.; Robinson, C. V.; Ruotolo, B. T. *Chem. Phys. Lett.* **2012**, *524*, 1–9.
(46) Pierson, N. A.; Valentine, S. J.; Clemmer, D. E. *J. Phys. Chem. B* **2010**, *114*, 7777–7783.
(47) Harvey, S. R.; Yan, J.; Brown, J. M.; Hoyes, E.; Wysocki, V. H. *Anal. Chem.* **2016**, *88*, 1218–1221.
(48) Kemper, P. R.; Dupuis, N. F.; Bowers, M. T. *Int. J. Mass Spectrom.* **2009**, *287*, 46–57.
(49) Deng, L.; Ibrahim, Y. M.; Baker, E. S.; Aly, N. A.; Hamid, A. M.; Zhang, X.; Zheng, X.; Garimella, S. V. B.; Webb, I. K.; Prost, S. A.; Sandoval, J. A.; Norheim, R. V.; Anderson, G. A.; Tolmachev, A. V.; Smith, R. D. *ChemistrySelect* **2016**, *1*, 2396–2399.
(50) Dugourd, P.; Hudgins, R. R.; Clemmer, D. E.; Jarrold, M. F. *Rev. Sci. Instrum.* **1997**, *68*, 1122–1129.
(51) McLuckey, S. A.; Goeringer, D. E. *Anal. Chem.* **1995**, *67*, 2493–2497.

(52) Mason, E. A.; McDaniel, E. W. *Transport Properties of Ions in Gases*, pg. 149.; Wiley: New York, 1988.
(53) Shelimov, K. B.; Clemmer, D. E.; Hudgins, R. R.; Jarrold, M. F. *J. Am. Chem. Soc.* **1997**, *119*, 2240–2248.
(54) Badman, E. R.; Hoaglund-Hyzer, C. S.; Clemmer, D. E. *Anal. Chem.* **2001**, *73*, 6000–6007.
(55) Revercomb, H. E.; Mason, E. A. *Anal. Chem.* **1975**, *47*, 970–983.

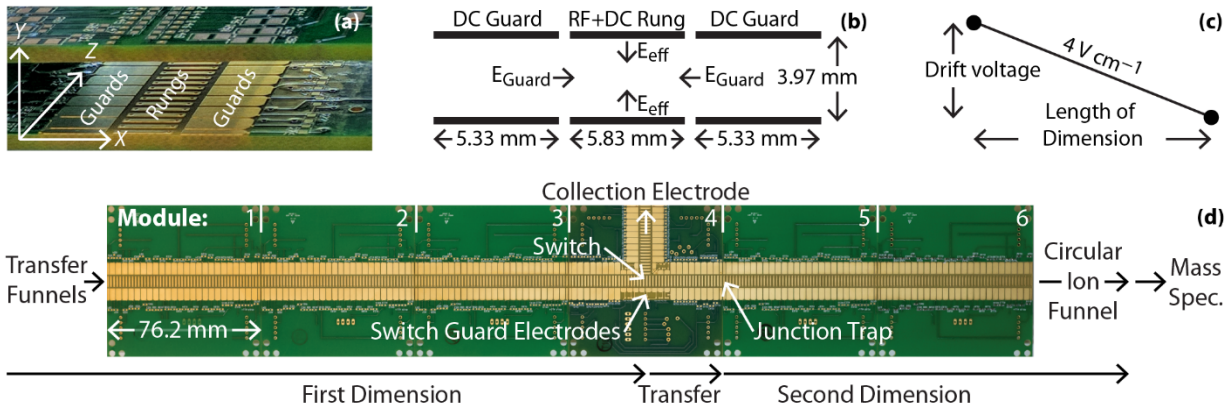

Figure 1. (a) Picture of a pair of SLIM boards forming a module. (b) Electrode dimensions and the electrostatic (E_{Guard}) and effective potential (E_{eff}) fields acting on the ions. (c) The 4 V cm^{-1} drift field used to separate ions is established by applying a monotonically decreasing DC potential to each subsequent rung electrode;[30] this implementation of SLIM does not use traveling waves. (d) Picture of the array of modules used in these experiments. Ions exiting the transfer funnels (post-trapping region of the ion funnel trap and the rectangular ion funnel) pass through three linear modules (numbered 1 to 3) and a tee module (4). Time-dependent voltages applied to the switch guard electrodes are used to either transmit ions entering the switch along the collinear path to the second dimension or divert those ions down the orthogonal path to a collection electrode. A junction trap between modules 4 and 5 is generated by biasing module 5 by +10 V relative to module 4. After the release of ions from the junction trap, ions pass through two linear modules (5 and 6) and a circular ion funnel before transfer to the mass spectrometer.

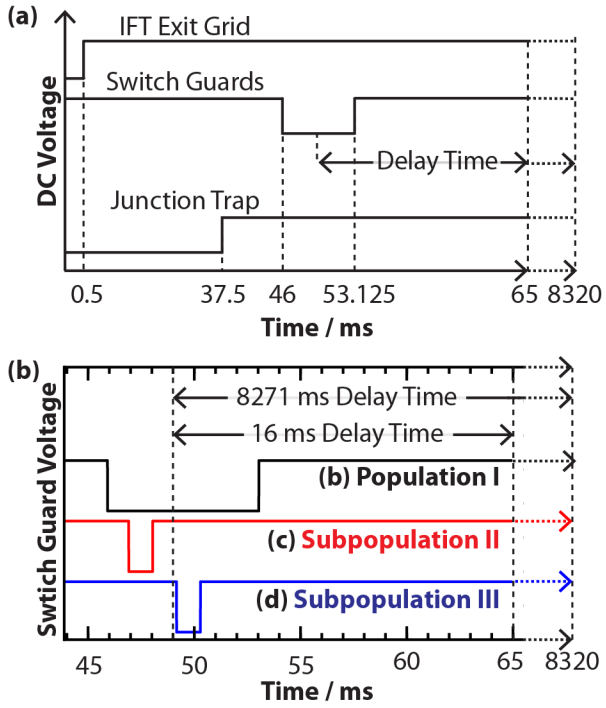

Figure 2. (a) Time-dependent voltages in tandem IM experiments. The ion funnel trap (IFT) exit grid is used to release a packet of ions for the first dimension of IM separation. The switch guard voltages of the SLIM Tee are lowered for some time (transmission window) to enable selection of a specific range of drift times. The junction trap voltage is raised prior to selection to prepare for ion accumulation at the junction trap. After selection, ions are accumulated and trapped in the junction trap for a delay time. The delay time is varied to enable time-dependent trapping of ions. After the delay time, the junction trap is lowered and ions undergo the second dimension of IM separation. The specific times in this panel correspond to the experimental parameters used to select and trap 7+ cytochrome *c* (Figure 4). Population I (b), subpopulation II (c), or subpopulation III (d) were selected depending on the voltage profile applied to the switch guard. The actual time differences between ion selection and the beginning of the second dimension are slightly different (up to 2 ms) in the three experiments and depend on the mobilities of the ions that are selected. For simplicity, a common delay time is reported for experiments probing the three populations.

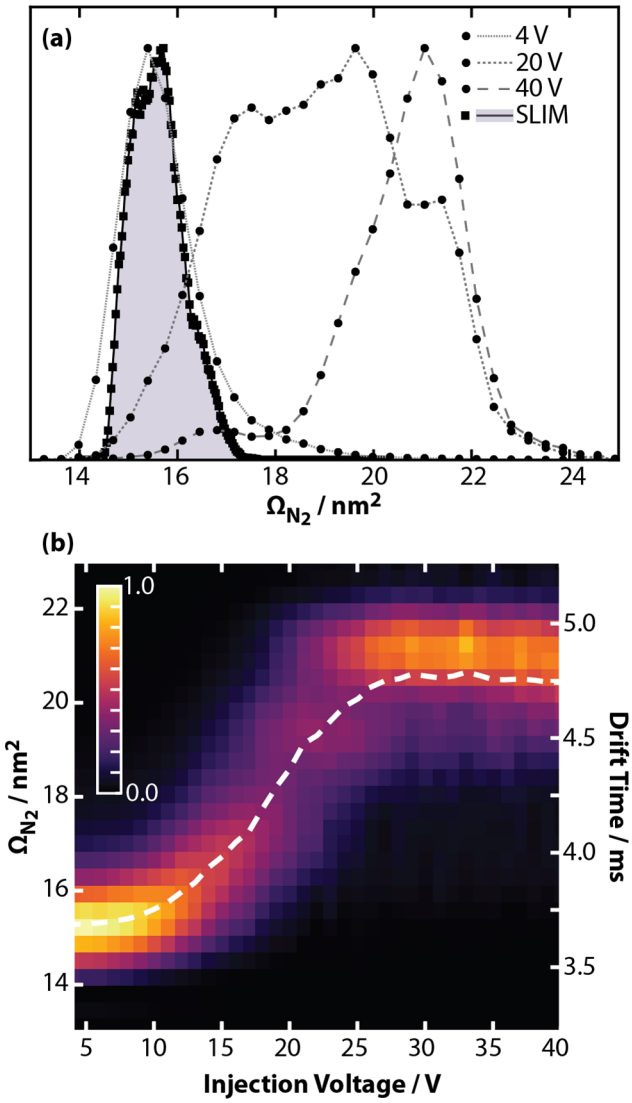

Figure 3. Apparent *Ω* distributions of 7+ cytochrome *c* acquired on a Waters Synapt G2 HDMS containing an RF-confining drift cell (*circles*, *grey dashed lines*). Three different *Ω* distributions were acquired at injection voltages of 4, 20, and 40 V into the Trap Cell; the extent of collision-induced unfolding (CIU) increases with the injection voltage. The *Ω* distribution acquired using SLIM (*squares*, *shaded distribution*) is also plotted. (b) Heat map of *Ω* versus injection voltage acquired using the RF-confining drift cell. The white dashed line shows the median value of the *Ω* distribution at each injection voltage.

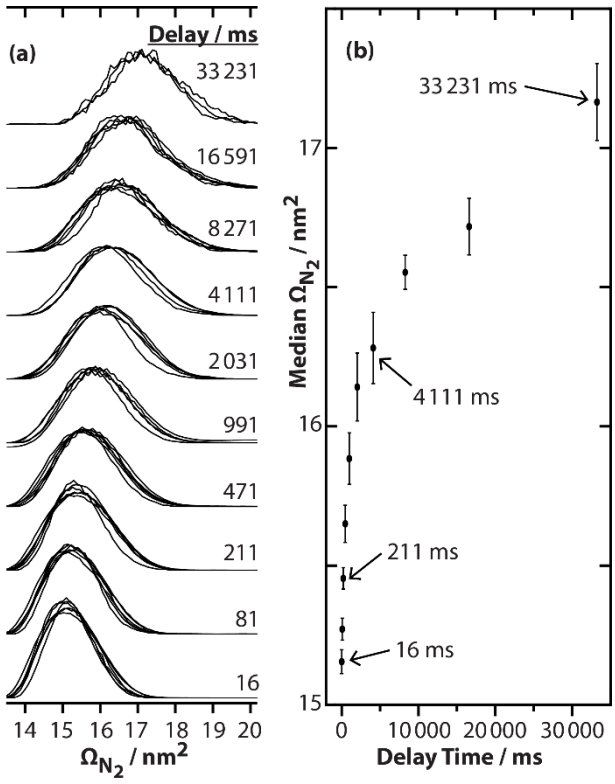

Figure 4. (a) Apparent *Ω* distributions of native-like, 7+ cytochrome *c* determined using selection-trapping experiments (Figure 1) as a function of delay time. Traces from replicate measurements performed on different days are included to illustrate the precision of the measurement. (b) The average of the median *Ω* values, based on analysis of the CDF (Figure S2) of each *Ω* distribution, are plotted versus delay times. The bars span the 90% confidence interval.

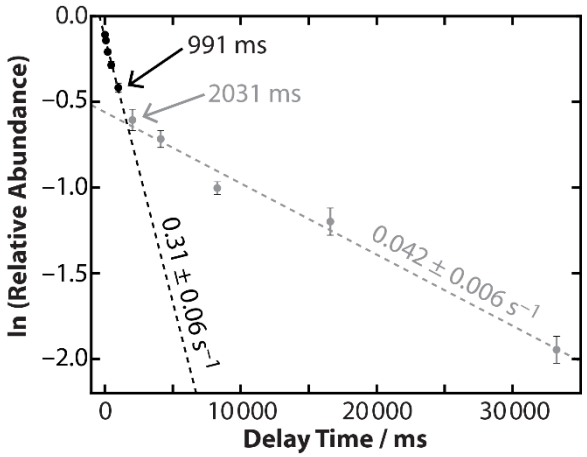

Figure 5. Plot of natural logarithm of the relative intensity of the initial population. The initial population is defined as ions that have Ω between 14.14 and 16.32 nm^2, which respectively correspond to 5% and 95% of CDF determined using a delay time of 16 ms. The rates of depletion are determined from the slopes of linear functions, which were fit to the results for delay times ranging from 16 to 911 ms (*black dashed line*, $R^2 = 0.979$) and from 2031 to 33 231 ms (*grey dashed line*, $R^2 = 0.987$). Markers represent the average of technical replicates, the bars span the standard error, and the reported rates span the 90% confidence interval.

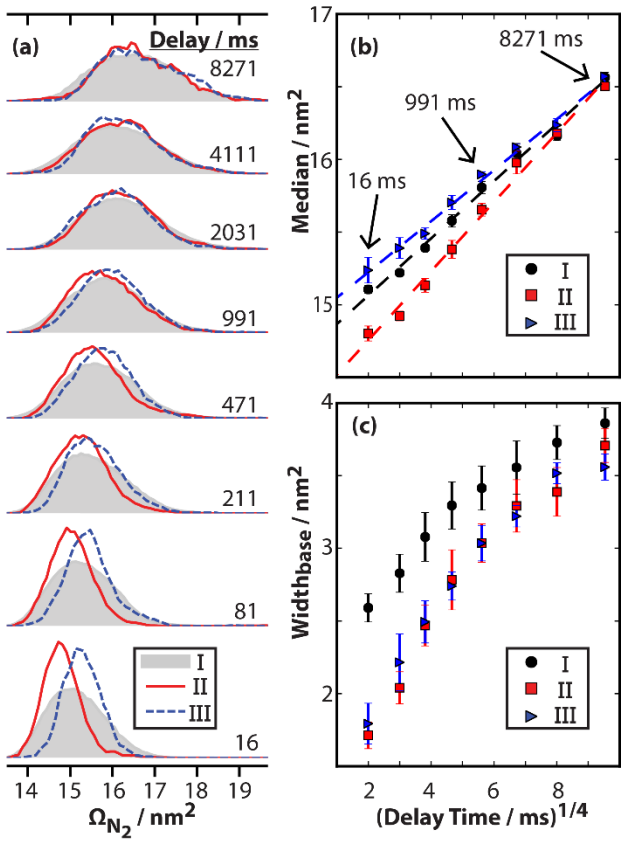

Figure 6. (a) Apparent *Ω* distributions determined from selection-trapping experiments of native-like, 7+ cytochrome *c* ions at delay times ranging from 16 to 8271 ms. A transmission window of 7.125 ms was used to select the entire population (**I**, *shaded distribution*) and a transmission window of 1.125 ms was used to select subpopulations (**II**, *red solid line*, and **III**, *blue dashed line*). All distributions are normalized to an integral of one. (b) Median *Ω* of population **I** (*black circles*), subpopulation **II** (*red squares*), and subpopulation **III** (*blue triangles*) plotted versus the fourth root of delay time, which was chosen arbitrarily to aid in visualization. (b) The apparent width at base of the *Ω* distributions for the three populations. For comparison, an apparent width of 0.69 nm^2 is expected for a single structure. Markers represent the average of technical replicates and the bars span the standard error.

For TOC only.

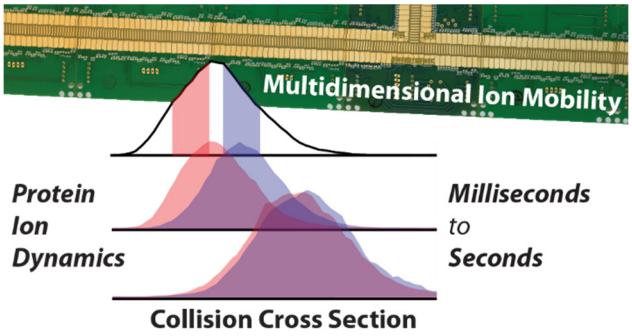
Multidimensional Ion Mobility
Protein
Ion
Dynamics
Milliseconds
to
Seconds
Collision Cross Section